Journal of Biomechanics 88 (2019) 201–208

Contents lists available at ScienceDirect

Journal of Biomechanics

journal homepage: www.elsevier.com/locate/jbiomech
www.JBiomech.com

Short communication

Sensitivity of multifrequency magnetic resonance elastography and diffusion-weighted imaging to cellular and stromal integrity of liver tissue

Angela Ariza de Schellenberger [a], Heiko Tzschätzsch [a], Baptiste Polchlopek [a], Gergely Bertalan [a], Felix Schrank [a], Karolina Garczynska [a], Paul A. Janmey [b], Jürgen Braun [c], Ingolf Sack [a,*]

[a] Department of Radiology, Charité – Universitätsmedizin Berlin, Germany
[b] Institute for Medicine and Engineering, University of Pennsylvania, Philadelphia, PA, USA
[c] Institute of Medical Informatics, Charité – Universitätsmedizin Berlin, Germany

ARTICLE INFO

Article history:
Accepted 27 March 2019

Keywords:
Liver microarchitecture
Freeze-thaw cycles
Viscoelasticity
Water diffusion
Magnetic resonance elastography
Diffusion-weighted imaging
Tabletop MRE

ABSTRACT

Microscopic structural alterations of liver tissue induced by freeze-thaw cycles give rise to palpable property changes. However, the underlying damage to tissue architecture is difficult to quantify histologically, and published data on macroscopic changes in biophysical properties are sparse.

To better understand the influence of hepatic cells and stroma on global biophysical parameters, we studied rat liver specimens freshly taken (within 30 min after death) and treated by freeze-thaw cycles overnight at either −20 °C or −80 °C using diffusion-weighted imaging (DWI) and multifrequency magnetic resonance elastography (MRE) performed at 0.5 T in a tabletop MRE scanner. Tissue structure was analyzed histologically and rheologic data were analyzed using fractional order derivatives conceptualized by a called *spring-pot* component that interpolates between pure elastic and viscous responses.

Overnight freezing and thawing induced membrane disruptions and cell detachment in the space of Disse, resulting in a markedly lower shear modulus μ and apparent diffusion coefficient (ADC) ($\mu[-20\,°C] = 1.23 \pm 0.73$ kPa, $\mu[-80\,°C] = 0.66 \pm 0.75$ kPa; $ADC[-20\,°C] = 0.649 \pm 0.028\ \mu m^2/s$, $ADC[-80\,°C] = 0.626 \pm 0.025\ \mu m^2/s$) compared to normal tissue ($\mu = 9.92 \pm 3.30$ kPa, $ADC = 0.770 \pm 0.023\ \mu m^2/s$, all $p < 0.001$). Furthermore, we analyzed the springpot-powerlaw coefficient and observed a reduction in −20 °C specimens (0.22 ± 0.14) compared to native tissue (0.40 ± 0.10, $p = 0.033$) and −80 °C specimens (0.54 ± 0.22, $p = 0.002$), that correlated with histological observations of sinusoidal dilation and collagen distortion within the space of Disse. Overall, the results suggest that shear modulus and water diffusion in liver tissue markedly decrease due to cell membrane degradation and cell detachment while viscosity-related properties appear to be more sensitive to distorted stromal and microvascular architecture.

© 2019 Published by Elsevier Ltd.

1. Introduction

Liver parenchyma is a cell-rich tissue whose major functions are determined by the interaction of hepatocytes, microvasculature, and extracellular matrix (ECM). Hepatocytes are organized in hepatic plates separated by sinusoids. The structure between a hepatocyte and a sinusoid is called the space of Disse. The sinusoidal vessels are irregular spaces between the hepatic plates, which are lined by sinusoidal endothelial cells (SEC), Kupffer cells, and collagen-based reticulin fibers. Alterations in sinusoidal vessels can precede fibrosis and promote hepatic stellate cell activation (Natarajan et al., 2017).

Magnetic resonance elastography (MRE) and water diffusion-weighted imaging (DWI) are two magnetic resonance imaging (MRI) methods that provide quantitative and microstructural information (Sack and Schaeffter, 2018). While MRE measures shear viscoelasticity, DWI quantifies the mean free path length traveled by water molecules in soft tissues (Hirsch et al., 2017).

Studies have correlated in vivo elastography data with histological markers to identify biophysical patterns associated with specific pathologies (Lupsor et al., 2008; Sack et al., 2013; Sandrini et al., 2014). For example, collagen accumulation leads to an increase in the liver shear modulus by an order of magnitude suggesting that elastography is sensitive to ECM remodeling (Georges et al., 2007;

* Corresponding author at: Charité – Universitätsmedizin Berlin, Department of Radiology, Charitéplatz 1, 10117 Berlin, Germany.
E-mail address: ingolf.sack@charite.de (I. Sack).

https://doi.org/10.1016/j.jbiomech.2019.03.037
0021-9290/© 2019 Published by Elsevier Ltd.

Reiter et al., 2014; Venkatesh et al., 2013). Complementarily, the DWI signal sensitively changes when the permeability of cell membranes is affected (Le Bihan, 2013). However, effects of cellular changes on viscoelastic parameters or effects of ECM alterations on the DWI signal require further study (Sack and Schaeffter, 2018; Van Beers et al., 2015).

The liver's microstructure can also be modulated by freeze-thaw cycles, which result in cell dehydration and disruption of cell membranes (Bakhach, 2009; Bischof et al., 1993; Li et al., 2018; Lu et al., 2014; Wex et al., 2014). Temperatures below 4 °C can already induce significant structural distortions such as SEC detachment from the space of Disse (Jain et al., 2004; Natarajan et al., 2017).

Although freezing-thawing of liver tissue induces palpable mechanical property changes, the underlying microscopic changes are difficult to quantify by conventional histological methods. Published data on freezing-induced mechanical property changes in liver tissue are sparse and partially conflicting (Lu et al., 2014; Lu and Untaroiu, 2013; Wex et al., 2014). Therefore, we combine MRE, DWI, and histological analysis to study fresh liver specimens from rats subjected to different freezing scenarios.

2. Materials and methods

Overall, 46 liver specimens from Wistar rats (3–4 months old) were investigated: native tissue (n = 11, MRE; n = 6, DWI), −20 °C-frozen/thawed tissue (n = 11, MRE; n = 6, DWI), −80 °C-frozen/thawed tissue (n = 6, MRE; n = 6, DWI). Cylindrical samples measuring 8 mm in height and diameter were chopped from the freshly harvested livers and investigated within 30 min or frozen overnight by temperature shock (approx. 12 h) at −20° or −80 °C and investigated after being fully thawed (approx. 2 h) at room temperature. Of note, both freezing procedures were identical in terms of sample sizes and freezing time. To avoid tissue deteriora-

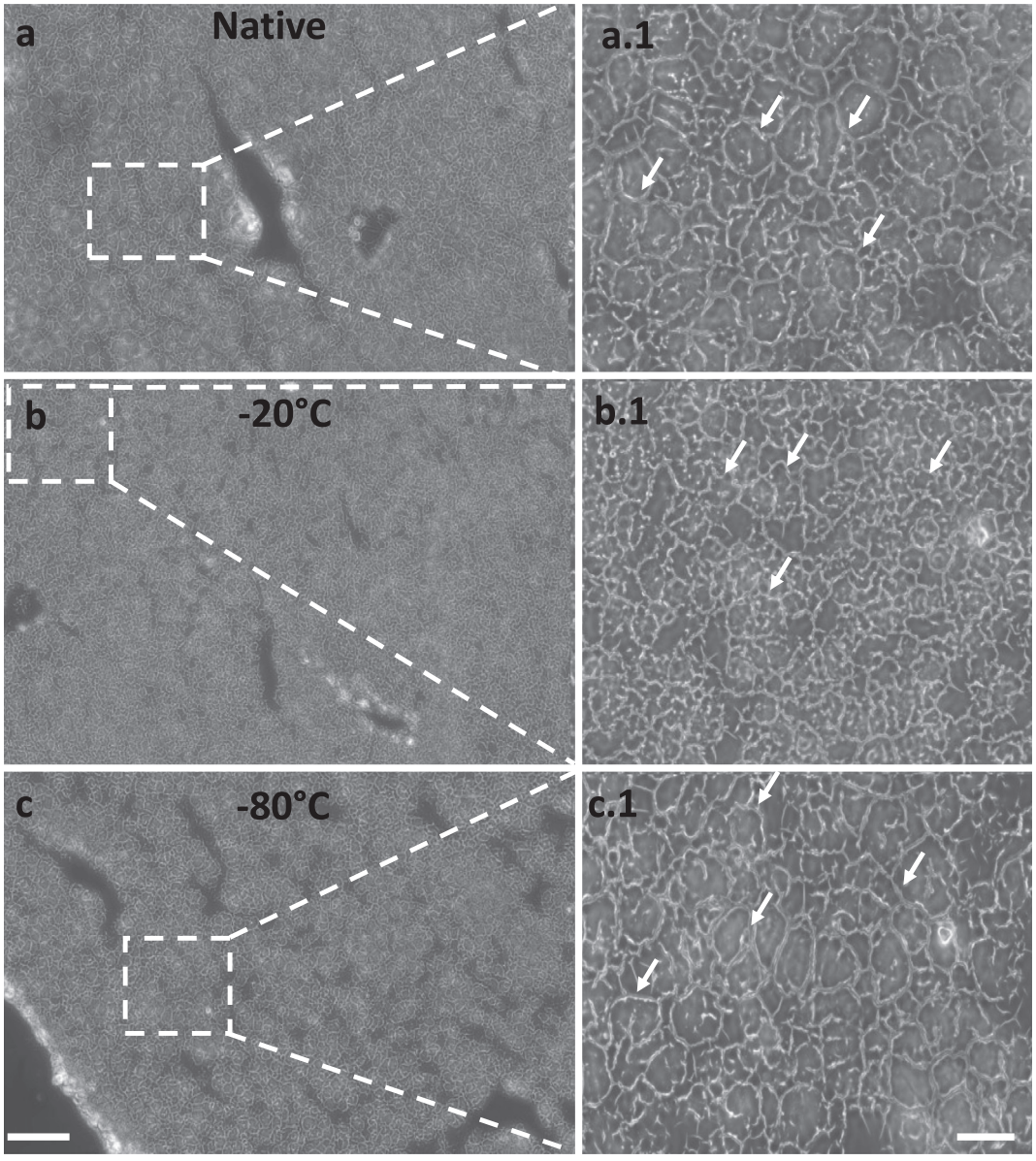

Fig. 1. Unstained cryosections of liver tissue of 5-μm thickness imaged with phase-contrast microscopy. ECM molecules such as collagen and elastin fibers are identified by their light diffraction properties (arrows). Liver frozen-thawed at −20 °C (b, b.1) shows significant distortions of tissue architecture and ECM while liver frozen at −80 °C (c, c.1) shows similar patterns as seen in native tissue (a, a.1). All scale bars correspond to 50 μm.

tion between successive measurements, each specimen was examined by either MRE or DWI.

2.1. Magnetic resonance elastography

A 0.5-T compact tabletop MRI device (Pure Devices GmbH, Würzburg, Germany) was used for all MRE and DWI examinations. For MRE, a customized spin-echo imaging sequence and piezoelectric driver were used as detailed in (Braun et al., 2018) and in Supplementary Materials.

For each driving frequency of 300, 400, 500, 600, 700, 800, 1000 and 1200 Hz, the acquired phase data were unwrapped and Fourier-transformed in time to extract complex-valued wave images. Wave images were fitted by an analytical solution based on Bessel functions prescribed in a z-infinite cylinder (Braun et al., 2018). The viscoelastic springpot model, which is a two-parameter fractional element, was fitted on shear-wave-speed over frequency, yielding a frequency-independent shear modulus μ and powerlaw exponent α (Braun et al., 2018),

$$c(\omega) = \sqrt{\frac{\mu^{1-\alpha}\eta^{\alpha}\omega^{\alpha}}{\rho}}\frac{1}{\cos\left(\frac{\pi}{4}\alpha\right)} \tag{1}$$

with specific viscosity $\eta = 1$ Pa · s and the tissue's density $\rho = 1$ kg/L. Of note, the springpot fit has been applied to shear wave speed data over frequency to derive a surrogate of the shear modulus dispersion function similar to the method proposed by Testu et al. (2017). While μ represents the shear modulus or 'stiffness' of a material (in kPa), the dimensionless parameter α relates to the slope of the viscoelastic dispersion function.

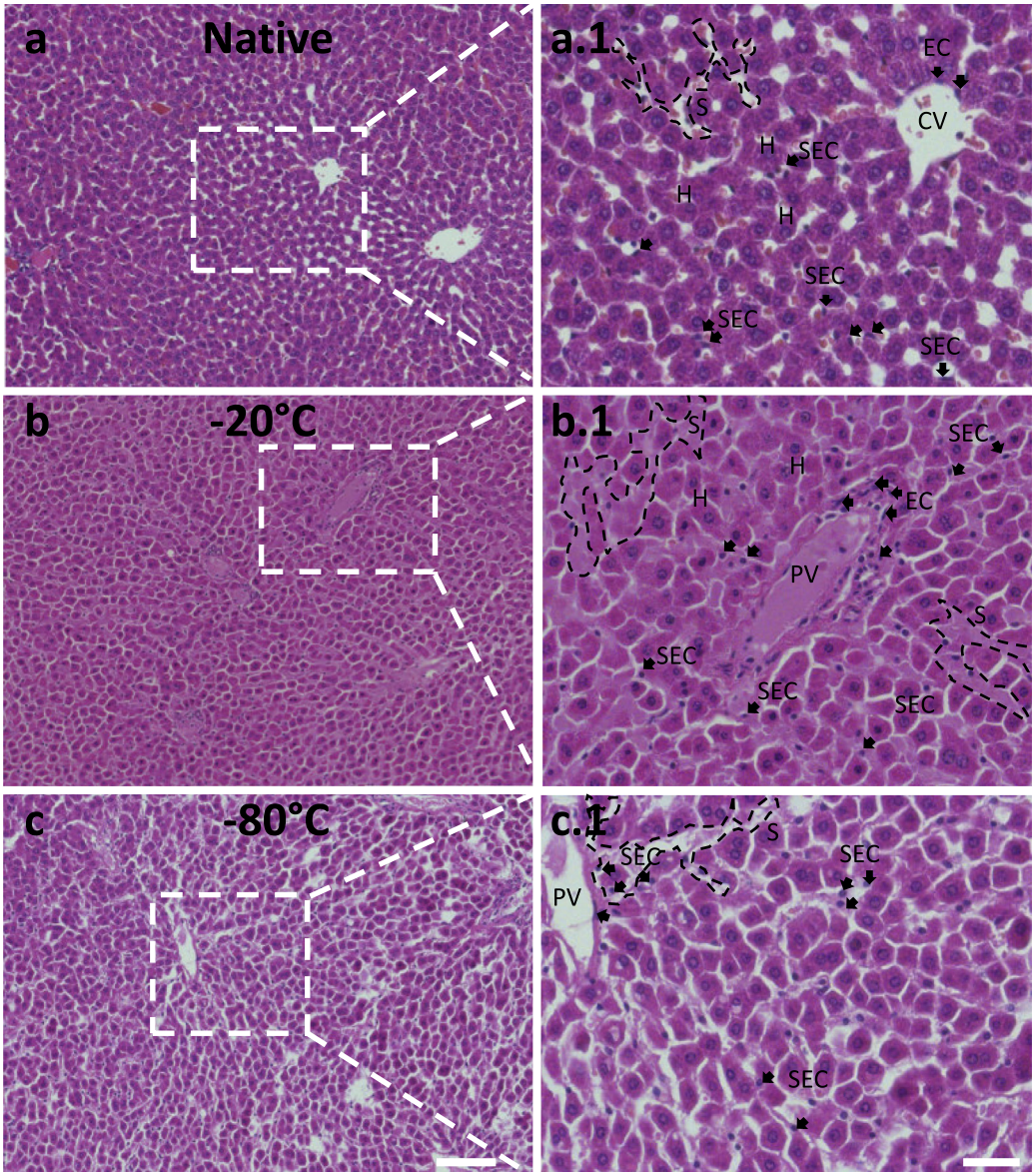

Fig. 2. H&E-stained liver sections of 5-μm thickness showing purple-blue cell nuclei, pink cell cytoplasm, and light pink sinusoids. Liver tissue after freezing-thawing at −20 °C (b, b.1) shows dilated sinusoids (– – – –) in comparison with samples frozen at −80 °C (c, c.1) and native samples (a. a-1). SEC nuclei appear roundish when detached from the space of Disse after freezing at either temperature (−20 °C and −80 °C) while native samples typically show elongated cell nuclei. All scale bars correspond to 50 μm. H (hepatocytes), SEC (sinusoidal endothelial cells), S (sinusoids), CV (central vein), PV (portal vein), EC (endothelial cells). (For interpretation of the references to color in this figure legend, the reader is referred to the web version of this article.)

2.2. Diffusion-weighted imaging

For DWI a customized spin-echo sequence with one pair of split diffusion gradients was applied to minimize long-term eddy currents while ensuring high b-values (Reese et al., 2003). Five b-values were sampled (50, 175, 300, 550, 675 and 800 s/mm^2) with diffusion weighting in the phase-encoding direction.

Detailed information on statistical analysis and histological characterization including microscopy and staining with hematoxylin and eosin (H&E), Masson's trichrome (MT), and pricosirius red (SR) are given in the Supplementary Material.

3. Results

3.1. Histological characterization

Our histological analysis revealed five principal effects of the freezing procedures on tissue microarchitecture:

(i) *Architectural distortion of liver stroma.* Phase microscopy as shown in Fig. 1 demonstrated increased tortuosity of sinusoidal structures, indicating stromal distortion at larger scale in tissue frozen at −20 °C.

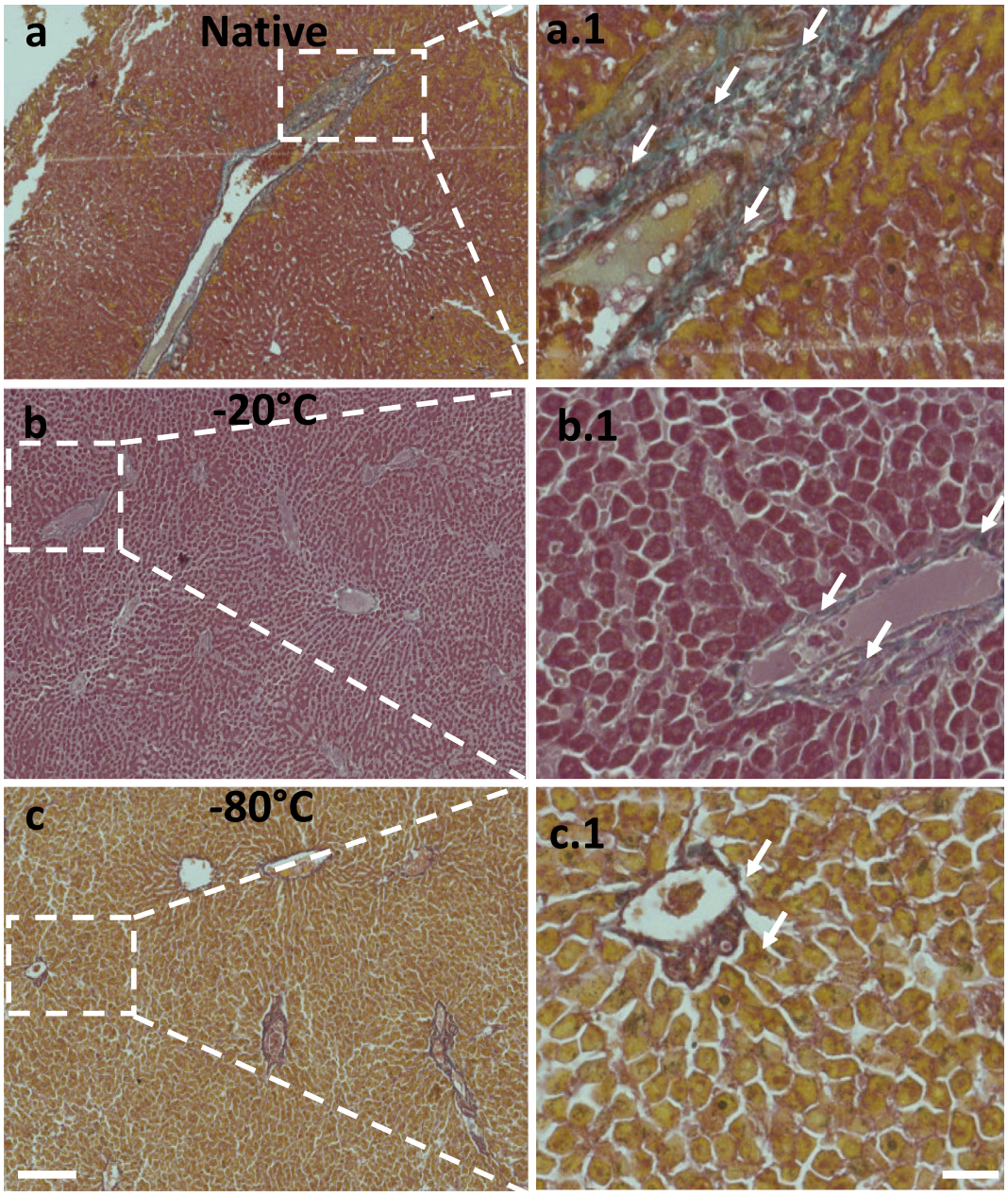

Fig. 3. Liver sections of 5-μm thickness stained with Masson's trichrome showing bright orange cell cytoplasm, black nuclei, orange-yellow erythrocytes, and green-blue collagen. Frozen-thawed tissue sections frozen at −20 °C (b, b.1) and −80 °C (c, c.1) show altered coloration indicating cell membrane disruption. Dilated sinusoids filled with a light pink color are observed at −20 °C only (b.1). The visible content of collagen surrounding vessel walls (arrows) is decreased due to freezing. All scale bars correspond to 50 μm. (For interpretation of the references to color in this figure legend, the reader is referred to the web version of this article.)

(ii) *Detachment of sinusoidal endothelial cells.* H&E stains as shown in Fig. 2 revealed detached endothelial cells (outside the space of Disse) and SEC (inside the space of Disse) by demonstrating rounded nuclei in frozen-thawed livers compared to more elongated nuclei in native livers.

(iii) *Sinusoidal dilation.* Fig. 2 demonstrates that sinusoids are enlarged in −20 °C specimens compared to −80 °C specimens.

(iv) *Disruption of hepatocyte membranes.* Differential uptake of MT dyes as shown in Fig. 3 indicates compromised membrane integrity of hepatocytes in samples treated with either freezing procedure. This is reflected by an altered coloration of hepatocytes (orange in native livers, dark pink in −20 °C livers and yellow in −80 °C livers).

(v) *Disruption of sinusoidal collagen.* Fig. 3 demonstrates absence of signals associated with collagen in vessel walls suggesting conformational distortions of collagen chains in frozen liver tissue samples. However, collagen near vessels walls became visible under fluorescent light in SR-stained samples as shown in Fig. 4, while collagen in the space of Disse remained absent in specimens frozen at −20 °C and appeared reduced in −80 °C samples.

Taken together, stromal architecture and sinusoidal integrity were preserved better at −80 °C than −20 °C. However, membrane disruption of hepatocytes, detachment of SEC, and collagen disruption in the space of Disse showed that both freezing procedures largely disrupt the cellular lattice between parenchyma (hepatocytes)

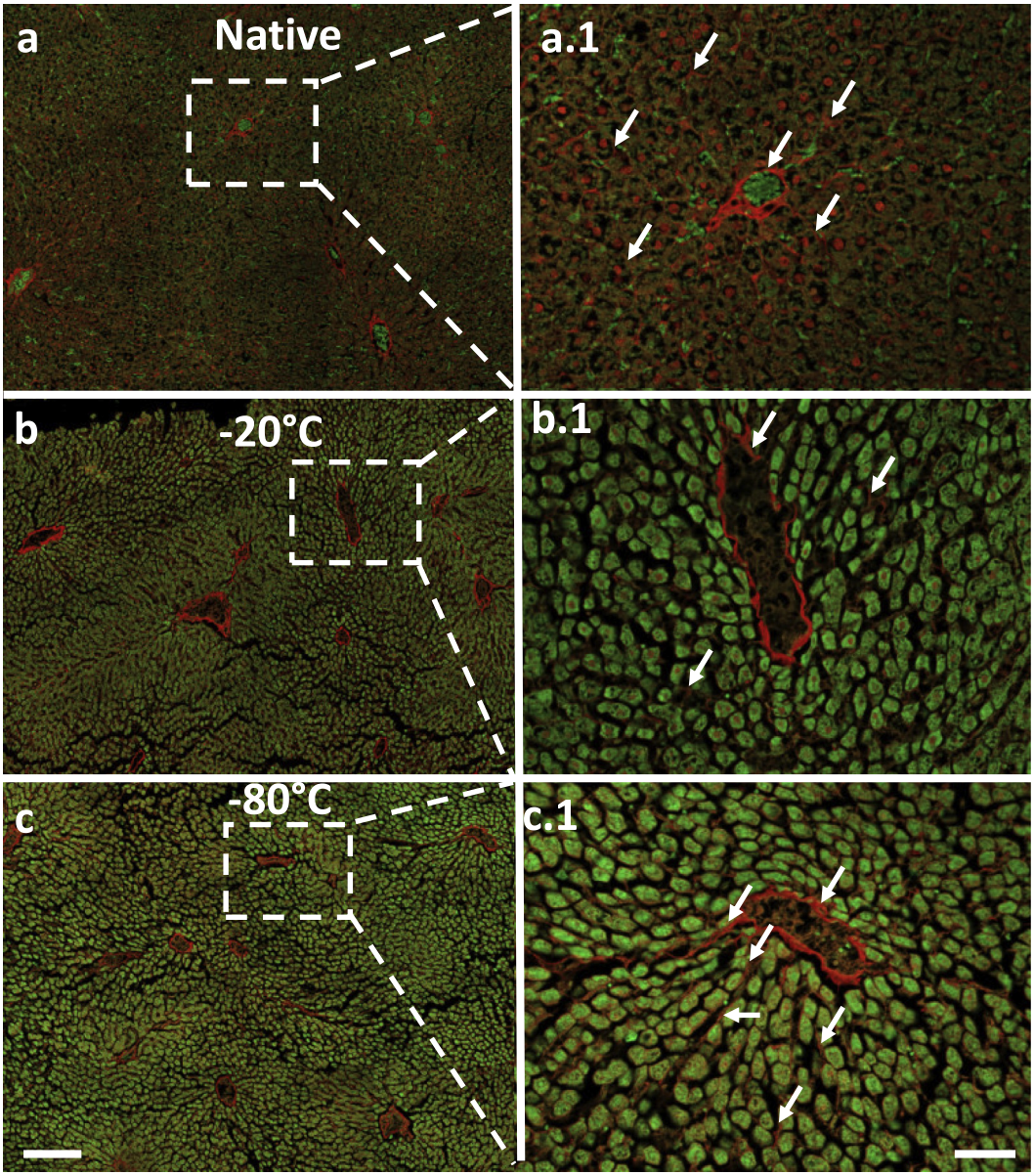

Fig. 4. SR-stained liver sections of 5-μm thickness for collagen detection. Collagen appears red against a green background in fluorescence microscopy. It is apparent that collagen surrounding vessel walls is well preserved in the frozen-thawed liver samples. However, the visibility of intercellular collagen in the space of Disse is reduced due to freezing in comparison with native tissue (a, a.1). No sinusoidal collagen is detectable in −20 °C samples (b, b.1) while little sinusoidal collagen is visible in livers frozen at −80 °C (c, c.1). (For interpretation of the references to color in this figure legend, the reader is referred to the web version of this article.)

and nonparenchymal cells (space of Disse). Our histological findings are summarized in Table 1.

3.2. MRE and DWI

A marked reduction of shear wave speed, averaged over vibration frequency, was measured in the frozen and then thawed tissue samples (native: 2.73 ± 0.26 m/s, −20 °C: 1.26 ± 0.20 m/s, −80 °C: 1.27 ± 0.16 m/s, all $p < 1 \times 10^{-9}$). The full group-averaged dispersion functions of shear wave speed (c) are shown in Fig. 5. The marked reduction in c by freezing-thawing is reflected in springpot shear modulus μ (native: 9.92 ± 3.30 kPa, −20 °C: 1.23 ± 0.73 kPa, −80 °C: 0.66 ± 0.75 kPa, all $p < 1 \times 10^{-7}$). The powerlaw exponent α was smaller in −20 °C specimens (0.22 ± 0.14) than in −80 °C specimens (0.54 ± 0.22, p = 0.002) and native livers (0.40 ± 0.10, p = 0.033) while there was no difference in α between −80 °C samples and native livers. Note, the higher relative change of μ compared to c relates to the square root function in Eq. (1) as well as the power of α in μ and ω. Group values and statistics are shown in Fig. 5.

The DWI-derived ADC was significantly reduced after freezing at −20 °C (0.649 ± 0.028 μm²/s) and at −80 °C (0.626 ± 0.025 μm²/s) in

Table 1
Major findings of histological analysis, MRE, and DWI in liver tissue after freezing-thawing at −20 °C and at −80 °C in comparison with native specimens (non-frozen, fresh livers). The significance level of histological observations was qualitatively assessed and is indicated by plus signs (ns: not significant, no change; +: minor increase/trend; ++: significant increase; +++: very pronounced and significant increase) while MRE and DWI values were statistically analyzed using the Kruskal-Wallis test with Bonferroni correction (– : decrease p < 0.05, —: decrease p < 0.001).

Method	Observation/parameter	−20 °C vs. native	−80 °C vs. native
Phase microscopy	Architectural distortion of liver stroma	++	ns
Hematoxylin and eosin (H&E)	Sinusoidal dilation	+++	+
	Detachment of SEC	+++	+++
Masson's trichrome (MT)	Collagen distortions in vessel walls	ns	ns
	Disrupted hepatocyte membrane	++	++
Sirius red (SR)	Collagen distortions at vessel walls	ns	ns
	Collagen distortions in space of Disse	+++	+
MRE	Elasticity (springpot μ)	—	—
MRE	Viscous dispersion (springpot α)	–	ns
DWI	ADC	—	—

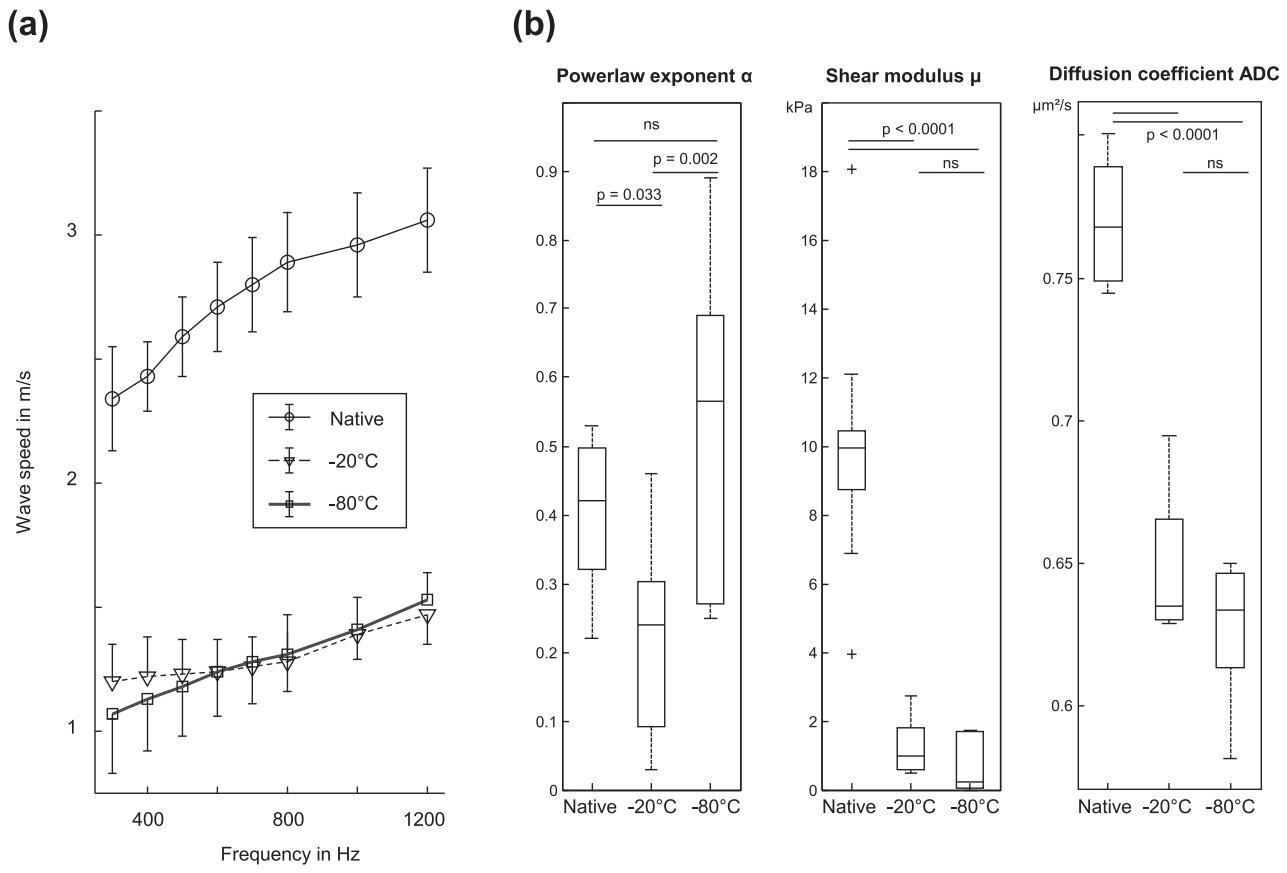

Fig. 5. Quantification of MRE and DWI in rat liver specimens in a native state (fresh tissue investigated within 30 min post mortem) and shock-frozen overnight at −20° and −80 °C directly after explant. (a) Group-mean values of shear wave speed over frequency. Error bars correspond to group standard deviations. (b) Frequency-independent group values of MRE according to Eq. (1) and DWI. MRE-derived powerlaw coefficient α and shear modulus μ of the viscoelastic springpot model represent the tissue's viscous dispersion behavior and elastic properties, respectively. The apparent diffusion coefficient (ADC) is derived from DWI.

Table 2
Mean values and standard deviation of MRE and DWI parameters.

Sample	c in m/s[+]	α	μ in kPa	ADC in μm²/s
Native	2.73 ± 0.26	0.4 ± 0.1	9.92 ± 3.3	0.770 ± 0.023
−20 °C	1.26[**] ± 0.20	0.22[*,++] ± 0.14	1.23[*] ± 0.73	0.649[**] ± 0.028
−80 °C	1.27[**] ± 0.16	0.54 ± 0.22	0.66[**] ± 0.75	0.626[**] ± 0.025

[**] $p < 0.001$ vs. native.
[*] $p < 0.05$ vs. native.
[++] $p < 0.01$ vs. −80 °C.
[+] Averaged over the entire frequency range.

comparison with native liver (0.770 ± 0.023 μm²/s). However, differences between the two freezing protocols were not significant (Fig. 5). All MRE and DWI values are summarized in Table 2.

4. Discussion

Water diffusion and viscoelasticity are complementary biophysical parameters that can be measured by MRI. Our study is the first to use compact MRI tailored for viscoelasticity and diffusion quantification in soft tissue samples for investigating microstructural changes in liver specimens induced by freezing-thawing cycles.

Our histological findings can readily be correlated with our macroscopically measured parameters by summarizing two key points: (i) cellular distortion such as disruption of membranes and reduced cellular adhesion is induced by freezing at both −80 °C or −20 °C, and (ii) stromal architectural distortion such as SEC detachment and sinusoidal dilation were induced mainly by −20 °C freezing. While (i) is mirrored by marked reductions of μ and ADC on the orders of 90% and 16%, respectively, (ii) is more subtle and is only reflected by a change in α while μ and ADC are not affected.

ADC is known to be sensitive to extracellular water and the permeability of cell membranes in our range of b-values of up to 1000 s/mm² (Le Bihan, 2013). The first consequence of ice crystal formation in the extracellular space is a change in chemical composition with an increase in ion concentration of the extracellular liquid. A concentration gradient therefore forms between the intra and the extracellular spaces, causing solutes to enter the cell and water to leave it (Bakhach, 2009). However, with shock temperature – as in our study – the flow of water into the extracellular medium is relatively low and intracellular crystallization predominates (Bakhach, 2009). This has major consequences for DWI and MRE: (i) The increase of ion concentration in the extracellular space reduces the mobility of water molecules and potentially lowers ADC (ii) Formation of intracellular ice crystals exerts a mechanical stress on cell membranes leading to disruption and detachment of hepatocytes (Mazur, 1977). Disruption of cell membranes potentially increases ADC-values by release of intracellular water (Li et al., 2018) while it decreases shear modulus. The reduction of ADC observed in our study points towards (i) or, alternatively, reflects deteriorations of fresh tissue (<30 min post-mortem) over time in addition to freezing. Irrespective the underlying nature of reduced water mobility, the observed reduction in ADC combined with our histological analysis suggests the dominant role of cellular integrity for the macroscopic shear modulus in normal rat livers.

However, it is important to mention that this conclusion applies to the dynamic range of 300–1200 Hz used in our experiments. Despite the fact that our springpot-derived parameters are, in principle, independent of frequency, viscous dispersion of shear wave speed or complex shear modulus in biological tissues is always sensitive to the velocity with which tissue elements are displaced, since actual biological tissue viscoelasticity differs from a perfect powerlaw function (Klatt et al., 2010). Therefore, we expect that sensitivity of viscous dispersion-related parameters (such as our parameter α) to ECM interactions might differ from our observations when measured in a different frequency range. Nonetheless, our principal findings might be extrapolated to the frequency range of in vivo elastography given the reported powerlaw behavior of liver specimens in overlapping frequency ranges between 25 and 1200 Hz (Reiter et al., 2014; Riek et al., 2011).

A further limitation of our study is that we only analyzed normal rat livers characterized by a relatively low ECM volume fraction (Blouin et al., 1977). When fibrotic liver is examined, in which the amount of ECM is significantly larger, our MRE and DWI values might be less markedly affected by cellular contributions. It would be interesting to see how shear modulus and water diffusion in fibrotic livers change due to freezing-thawing cycles. We expect that freezing fibrotic livers has less effect on μ and ADC than freezing normal livers, while α is expected to be more sensitive to freezing when the amount of ECM is pathologically increased. In future studies, analysis of fibrillar organization of ECM components could be improved by label-free microscopy exploiting second harmonic generation (Couture et al., 2015; Liu et al., 2017), spatial light interference microscopy or quantitative phase imaging (Majeed et al., 2017). In any case, combining biophysically based quantitative MRI with histological analysis in frozen tissues provides a wealth of information that is relevant for the interpretation of clinical in vivo imaging markers in health and disease.

In summary, compact tabletop MRI and histological analyses were combined to investigate the cellular and extracellular contributions to macroscopic shear modulus and water diffusion in normal rat liver specimens treated by freezing-thawing cycles. We found that deterioration of cell membranes and SEC detachment reduced the macroscopic shear modulus and water diffusion coefficient. Distortion of sinusoidal collagen and sinusoidal dilation after −20 °C freezing were associated with reduction of the viscous dispersion-related springpot-powerlaw coefficient in the frequency range of 300–1200 Hz. Our study contributes to the understanding of how the microarchitecture of liver tissue influences macroscopic shear elastic and shear viscous tissue properties and facilitates the interpretation of quantitative biophysical MRI markers in future diagnostic applications.

Conflict of interest

None of the authors declares a conflict of interest.

Acknowledgement

Support of the German Research Foundation (GRK2260, BIOQIC and SFB1340 Matrix-in-Vision), the German Federal Ministry of Education and Research (LiSyM 031L0057) and of the European Union's Horizon 2020 Program (ID 668039, EU FORCE – Imaging the Force of Cancer) is gratefully acknowledged.

Appendix A. Supplementary material

Supplementary data to this article can be found online at https://doi.org/10.1016/j.jbiomech.2019.03.037.

References

Bakhach, J., 2009. The cryopreservation of composite tissues: principles and recent advancement on cryopreservation of different type of tissues. Organogenesis 5, 119–126.

Bischof, J., Christov, K., Rubinsky, B., 1993. A morphological study of cooling rate response in normal and neoplastic human liver tissue: cryosurgical implications. Cryobiology 30, 482–492.

Blouin, A., Bolender, R.P., Weibel, E.R., 1977. Distribution of organelles and membranes between hepatocytes and nonhepatocytes in the rat liver parenchyma. A stereological study. J. Cell. Biol. 72, 441–455.

Braun, J., Tzschatzsch, H., Korting, C., Ariza de Schellenberger, A., Jenderka, M., Driessle, T., Ledwig, M., Sack, I., 2018. A compact 0.5 T MR elastography device and its application for studying viscoelasticity changes in biological tissues during progressive formalin fixation. Magn. Reson. Med. 79, 470–478.

Couture, C.A., Bancelin, S., Van der Kolk, J., Popov, K., Rivard, M., Legare, K., Martel, G., Richard, H., Brown, C., Laverty, S., Ramunno, L., Legare, F., 2015. The impact of collagen fibril polarity on second harmonic generation microscopy. Biophys. J. 109, 2501–2510.

Georges, P.C., Hui, J.J., Gombos, Z., McCormick, M.E., Wang, A.Y., Uemura, M., Mick, R., Janmey, P.A., Furth, E.E., Wells, R.G., 2007. Increased stiffness of the rat liver precedes matrix deposition: implications for fibrosis. Am. J. Physiol. Gastrointest. Liver Physiol. 293, G1147–G1154.

Hirsch, S., Braun, J., Sack, I., 2017. Magnetic Resonance Elastography: Physical Background And Medical Applications. Wiley-VCH.

Jain, S., Xu, H., Duncan, H., Jones, J., Zhang, J., Clemens, M., Lee, C., 2004. Ex-vivo study of flow dynamics and endothelial cell structure during extended hypothermic machine perfusion preservation of livers. Cryobiology 48, 322–332.

Klatt, D., Friedrich, C., Korth, Y., Vogt, R., Braun, J., Sack, I., 2010. Viscoelastic properties of liver measured by oscillatory rheometry and multifrequency magnetic resonance elastography. Biorheology 47, 133–141.

Le Bihan, D., 2013. Apparent diffusion coefficient and beyond: what diffusion MR imaging can tell us about tissue structure. Radiology 268, 318–322.

Li, D., Zhu, Z., Sun, D.-W., 2018. Effects of freezing on cell structure of fresh cellular food materials: a review. Trends Food Sci. Technol.

Liu, Y., Keikhosravi, A., Mehta, G.S., Drifka, C.R., Eliceiri, K.W., 2017. Methods for quantifying fibrillar collagen alignment. Methods Mol. Biol. 1627, 429–451.

Lu, Y.C., Kemper, A.R., Untaroiu, C.D., 2014. Effect of storage on tensile material properties of bovine liver. J. Mech. Behav. Biomed. Mater. 29, 339–349.

Lu, Y.C., Untaroiu, C.D., 2013. Effect of storage methods on indentation-based material properties of abdominal organs. Proc. Inst. Mech. Eng. H 227, 293–301.

Lupsor, M., Badea, R., Stefanescu, H., Grigorescu, M., Sparchez, Z., Serban, A., Branda, H., Iancu, S., Maniu, A., 2008. Analysis of histopathological changes that influence liver stiffness in chronic hepatitis C. Results from a cohort of 324 patients. J. Gastrointestin. Liver Dis. 17, 155–163.

Majeed, H., Okoro, C., Kajdacsy-Balla, A., Toussaint, K.C., Popescu, G., 2017. Quantifying collagen fiber orientation in breast cancer using quantitative phase imaging. J. Biomed. Opt. 22, 46004.

Mazur, P., 1977. The role of intracellular freezing in the death of cells cooled at supraoptimal rates. Cryobiology 14, 251–272.

Natarajan, V., Harris, E.N., Kidambi, S., 2017. SECs (sinusoidal endothelial cells), liver microenvironment, and fibrosis. Biomed. Res. Int. 2017, 4097205.

Reese, T.G., Heid, O., Weisskoff, R.M., Wedeen, V.J., 2003. Reduction of eddy-current-induced distortion in diffusion MRI using a twice-refocused spin echo. Magn. Reson. Med. 49, 177–182.

Reiter, R., Freise, C., Jöhrens, K., Kamphues, C., Seehofer, D., Stockmann, M., Somasundaram, R., Asbach, P., Braun, J., Samani, A., Sack, I., 2014. Wideband MRE and static mechanical indentation of human liver specimen: sensitivity of viscoelastic constants to the alteration of tissue structure in hepatic fibrosis. J. Biomech. 47, 1665–1674.

Riek, K., Klatt, D., Nuzha, H., Mueller, S., Neumann, U., Sack, I., Braun, J., 2011. Wide-range dynamic magnetic resonance elastography. J. Biomech. 44, 1380–1386.

Sack, I., Joehrens, K., Wuerfel, E., Braun, J., 2013. Structure sensitive elastography: on the viscoelastic powerlaw behavior of in vivo human tissue in health and disease. Soft Matter 9, 5672–5680.

Sack, I., Schaeffter, T., 2018. Quantification of Biophysical Parameters in Medical Imaging. Springer, Heidelberg.

Sandrini, J., Boursier, J., Chaigneau, J., Sturm, N., Zarski, J.P., Le Bail, B., de Ledinghen, V., Cales, P., Rousselet, M.C., 2014. Quantification of portal-bridging fibrosis area more accurately reflects fibrosis stage and liver stiffness than whole fibrosis or perisinusoidal fibrosis areas in chronic hepatitis C. Mod. Pathol. 27, 1035–1045.

Testu, J., McGarry, M.D.J., Dittmann, F., Weaver, J.B., Paulsen, K.D., Sack, I., Van Houten, E.E.W., 2017. Viscoelastic power law parameters of in vivo human brain estimated by MR elastography. J. Mech. Behav. Biomed. Mater. 74, 333–341.

Van Beers, B.E., Daire, J.L., Garteiser, P., 2015. New imaging techniques for liver diseases. J. Hepatol. 62, 690–700.

Venkatesh, S.K., Yin, M., Ehman, R.L., 2013. Magnetic resonance elastography of liver: technique, analysis, and clinical applications. J. Magn. Reson. Imag. 37, 544–555.

Wex, C., Stoll, A., Frohlich, M., Arndt, S., Lippert, H., 2014. Mechanics of fresh, frozen-thawed and heated porcine liver tissue. Int. J. Hyperthermia 30, 271–283.